Polymer Chemistry

PAPER

View Article Online
View Journal | View Issue

Cite this: *Polym. Chem.*, 2015, **6**, 6340

Strong emission of 2,4,6-triphenylpyridine-functionalized polytyrosine and hydrogen-bonding interactions with poly(4-vinylpyridine)†

Mohamed Gamal Mohamed,[a] Fang-Hsien Lu,[a] Jin-Long Hong[a] and Shiao-Wei Kuo*[a,b,c]

Received 17th June 2015,
Accepted 18th July 2015

DOI: 10.1039/c5py00938c

www.rsc.org/polymers

In this paper 2,4,6-triphenyl pyridine-functionalized polytyrosine (Pyridine-PTyr) was successfully synthesized by living ring-opening polymerization where 2,6-bis(4-aminophenyl)-4-phenylpyridine (Pyridine-NH_2) was the initiator. The photo-physical characteristics of Pyridine-NH_2 and Pyridine-PTyr were elucidated *via* UV-vis absorption and photoluminescence spectra, revealing that unlike Pyridine-PTyr, Pyridine-NH_2 shows solvatochromic effects in solvents with different polarities. Additionally, Pyridine-NH_2 exhibited aggregation-caused quenching (ACQ) phenomena; however, it became an aggregation-induced emission (AIE) material after attachment to the rigid-rod conformation of polytyrosine. Based on differential scanning calorimetry results, we observed that after blending Pyridine-PTyr with P4VP a single glass transition temperature due to their miscibility through the intermolecular hydrogen bonding of the phenolic OH groups in the PTyr backbone and pyridine ring in P4VP was revealed, as indicated by IR spectroscopy. Obviously, the emission intensity of Pyridine-PTyr decreased after blending with P4VP with a hypsochromic shift from 536 to 489 nm, presumably due to the release of the restricted intramolecular rotation of the triphenyl pyridine unit in the center of the polymer and the polymer chains of Pyridine-PTyr became separated random coils based on WAXD results.

Introduction

Polypeptides are a class of amino acid-based polymers that have been received much attention from many researchers in recent years because of their potential application as biocompatible materials and their conformational transitions.[1–6] It is well established that there are three kinds of secondary structure of polypeptides in both the solution and bulk state, including α-helical, β-sheets and random coil.[7,8] The secondary structures of polypeptides are dependent on the degree of polymerization. For example if the degree of polymerization is higher than 18 the secondary structure of the polypeptides will be an α-helical structure, which can act as rigid-rod like polymers and it is stabilized through intramolecular hydrogen bonding interactions.[9] Synthetic polypeptides are carried out *via* the living-ring opening polymerization of *N*-carboxyanhydride [NCA] and versatile peptide monomers derivatives at room temperature with a controlled polydispersity index (PDI).[10,11] Much literature has reported that with the introduction of carbohydrates[12,13] and poly(ethylene oxide)[14,15] in the main or side chains of the polypeptide backbone these smart materials can behave as drug delivery and stimuli-responsive polymers.

Recently non-covalent interactions have played a crucial role in forming supramolecular complexes without any chemical reactions. Non-covalent interactions include hydrophobic interactions, dipole–dipole interactions, metal–ligand coordinations and hydrogen bonding interactions. In this report, we employed hydrogen bonding interactions as one of the most useful methods to form supramolecular complexes because of their moderate strength and reversibility.[19] Also, the addition of functional moieties to the main chain or a side chain of the polypeptides is another convenient method for improving the thermal or self-assembly behaviour of polypeptides.[16–18] For example, we concluded that the blending of poly(γ-benzyl-L-glutamate) (PBLG) with random-coil oligomers through intermolecular hydrogen bonding to hydrogen bond donor poly-

[a]*Department of Materials and Optoelectronic Science, National Sun Yat-Sen University, Kaohsiung, Taiwan*
[b]*Department of Medicinal and Applied Chemistry, Kaohsiung Medical University, Kaohsiung, Taiwan*
[c]*School of Chemical Engineering, East China University of Science and Technology, Shanghai, China. E-mail: kuosw@faculty.nsysu.edu.tw*

†Electronic supplementary information (ESI) available: Experimental detail of DSC, NMR, MS, GPC and fluorescence lifetime of Pyridine-NH_2 and Pyridine-PTyr behaviour. See DOI: 10.1039/c5py00938c

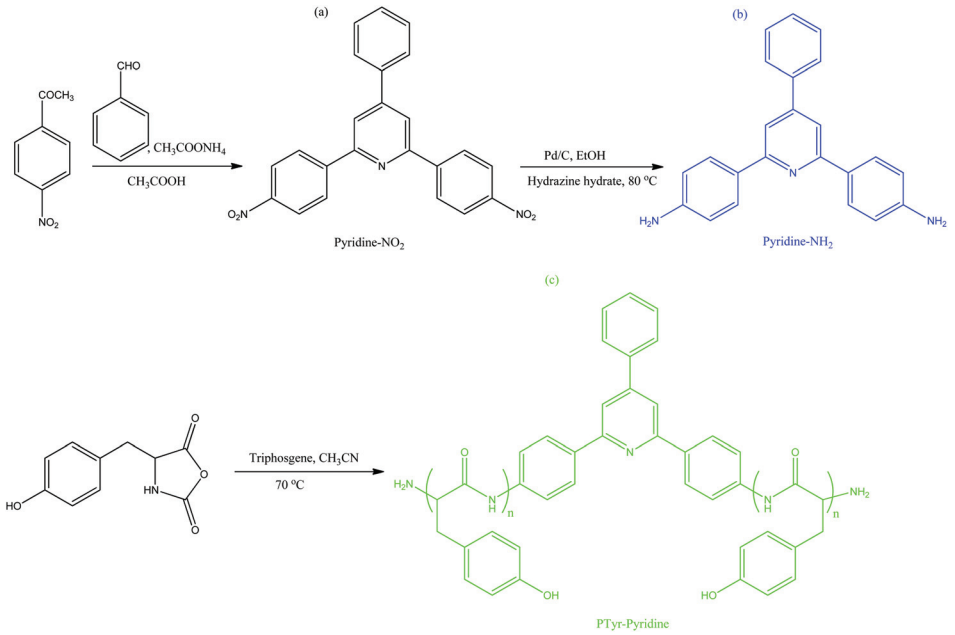

Scheme 1 Synthesis of (a) Pyridine-NO_2, (b) Pyridine-NH_2 and (c) Pyridine-PTyr.

mers and the secondary blending with other structures of PBLG altered the behaviour.[19,20] We also demonstrated the chain behavior of the PTyr–P4VP blend through intermolecular hydrogen bonding in MeOH and DMF solutions: inter-polymer complex aggregates and separated random coil based on FTIR spectroscopy and wide-angle X-ray diffraction analyses.[21]

Fluorescent-organic materials have been designed and have attracted attention in recent years due to their interesting potential optical applications in optoelectronic devices[22] and as fluorescence sensors.[23,24] However, the emission of most organic fluorescent materials (pyrene, carbazolyl and dansyl) becomes weak or non-emissive at high concentrations or in aggregated states due to their strong intermolecular π–π interaction;[25] this effect is known as aggregation-caused quenching (ACQ). This effect results in an increased possibility of π–π stacking leading to the formation of excimers and exciplexes in the excited state.[26] Therefore, to solve this problem, it is important to develop new fluorescent materials that emit more efficiently in the solid and aggregate states than as monomers in solution. Such materials are associated with two unusual phenomena that are the exact opposites of ACQ and identified by Tang *et al.*:[27] aggregation-induced emission (AIE)/aggregation-induced enhancement emission (AIEE) luminescent materials are weak or non-luminescent in the solution state, but they become strong emissive materials when they aggregate as nanoparticles in solution and in the condensed state. These researchers reported the first aggregation-induced emission (AIE) active compounds based on the pentaphenyl derivatives of silole that showed only a weak fluorescence in solution and were highly fluorescent after aggregation. These authors also reported that the mechanism of aggregation-induced emission is associated with the restriction of intramolecular rotation (RIR) of the fluorophore compound.[27] Additionally, Hong *et al.* reported AIE material's attachment to polypeptides through covalent chemical bonding and ionic interactions.[28] For example, Hong *et al.* designed two kinds of PBLG as TP1PBLG and TP2PBLG containing tetraphenylthiophene (TP) with aggregation-induced emission properties. These researchers found that the emission intensity of the TP unit in TP2PBLG decreased due to the intermolecular aggregate of the central TP unit in the TP2PBLG being sterically blocked by the large α-helical PBLG chains, leading to reduced AIEE.[28] Recently, they also reported that (*E*)-4-(2-(anthracen-9-yl)vinyl-pyridine (AnPy) blended with different amounts of polytyrosine through hydrogen bond interactions exhibits intramolecular charge transfer (ICT) and AIE properties at a low AnPy content.[29] Building on the studies described above, in this work, we successfully synthesized 2,6-bis(4-aminophenyl)-4-phenylpyridine (Pyridine-NH_2) as the initiator for the living ring-opening polymerization of L-tyrosine-*N*-carboxyanhydride (NCA) to obtain Pyridine-PTyr (Scheme 1). We used photoluminescence spectroscopy to investigate the fluorescence characteristics of Pyridine-NH_2 and Pyridine-PTyr. We expect that Pyridine-PTyr, possessing phenolic OH groups, will form intermolecular hydrogen bonds with poly(4-vinylpyridine) (P4VP) and may exhibit a separated coil behavior in this polymer blend in a *N*-dimethylformamide (DMF) solution. We used differential scanning calorimetry (DSC), Fourier transform infrared (FTIR) spectroscopy, UV-vis spectroscopy and photoluminescence spectroscopy to investigate the miscibility behavior, hydrogen bonding interactions and secondary structures of PTyr-Pyridine–P4VP blends.

Experimental section

Materials

Benzaldehyde, *p*-nitroacetophenone, ammonium acetate, and 10 wt% Pd/C (Merck) were used as received. DMF, ethanol and methanol were purchased from Merck, dried over calcium hydride overnight and distilled under reduced pressure. L-Tyrosine was purchased from MP Biomedicals. Triphosgene (TCI), P4VP (Aldrich, 160 000 g mol^{-1}), MeCN (Across, 99.5%), hexane (Across), MeOH (Across), dichloromethane (DCM), dimethylsulfoxide (DMSO), acetone, and tetrahydrofuran (THF) were purchased from Tedia. L-Tyrosine *N*-carboxyanhydride (Tyr-NCA) was prepared according to our previous study[21] and the synthesis of Pyridine-NO_2 has been reported previously.[30]

Synthesis of 2,6-bis(4-aminophenyl)-4-phenylpyridine (Pyridine-NH_2)[30]

A mixture of Pyridine-NO_2 (2.500 g, 0.012 mol) and 0.075 g of 10% Pd/C were dissolved in 60 mL of anhydrous ethanol. Then, the reaction mixture was heated to 90 °C for 3 h in a 150 mL two neck bottomed flask equipped with a stirring bar under N_2 atmosphere. After that, added dropwise of 20 mL of hydrazine monohydrate (in 20 mL of ethanol). The reaction mixture was heated to 80 °C overnight and then subsequently filtered to remove Pd/C. After cooling to room temperature, the yellow solid crystals were isolated by filtration, twice recrystallized from ethanol and vacuum-dried to obtain the product (1.50 g, 70%) that exhibits a melting point of 201 °C (DSC, Fig. S1†). The following peaks of the FTIR (KBr, cm^{-1}) spectrum were obtained: 3471 and 3379 cm^{-1} (N–H stretching), and 1620 cm^{-1} (N–H deformation). ^{1}H NMR obtained chemical shifts of (500 MHz, DMSO-d_6, δ, ppm): 6.71–8.04 (14H, Aromatic protons) and 5.42 (4H, NH_2) (Fig. S2†). The following chemical shifts were observed for ^{13}C NMR (125 MHz, DMSO-d_6, δ, ppm): 156.63, 149.89, 148.66, 138.59, 129.025, 127.79, 127.082, 126.59, 113.70 and 112.74. High resolution FT-MS $[M + H]^+$ m/z for ($C_{23}H_{19}N_3$): 338.17: calc.: 337.42 (Fig. S3†).

Synthesis of Pyridine-PTyr by ring opening polymerization (ROP) of Tyr-NCA

Tyr-NCA (3.00 g, 11.34 mmol) was weighed in a dry box under N_2, placed in a three-neck bottle and dissolved in anhydrous DMF (20 mL). The solution mixture was stirred for 15 min prior to the introduction of a solution of Pyridine-NH_2 (0.08 g, 0.23 mmol) in anhydrous DMF (3 mL) using a nitrogen purged syringe. After stirring for 72 h at 0 °C, the polymer was recovered through precipitation in diethyl ether (Et_2O) and subsequently dissolved in methanol and recovered through precipitation in ether. The polymer was purified three times from methanol/ether to give a pure yellow powder and dried under high vacuum at 30 °C. A yield of 2.5 g was obtained. The following peaks were obtained in FTIR (KBr, cm^{-1}) spectra: 3288 (NH), 1601, 1590, 753 and 698 (Ar). ^{1}H NMR chemical shifts were (500 MHz, DMSO-d6, δ, ppm): 2.90 (d, 2H, CH_2), 4.40 (t, 1H), 6.69 (d, 2H, Ar), 6.95 (d, 2H, Ar), 7.94 (s, 1H, NH) and 9.14 (s, 1H). M_n = 11 768 g mol^{-1}, PDI = 1.22 (GPC, Fig. S4†).

The preparation of Pyridine-PTyr with P4VP blending

Mixtures of Pyridine-PTyr–P4VP were prepared by dissolving various weight percentages of P4VP with Pyridine-Ptyr in DMF solutions; the solutions were then stirred for 2 days to generate intermolecular hydrogen bonding interactions. The solvent was then evaporated in a high vacuum at 60 °C for 72 h.

Characterization

^{1}H and ^{13}C nuclear magnetic resonance (NMR) spectra were obtained using an INOVA 500 instrument with DMSO-d_6 as the *d*-solvent and tetramethylsilane (TMS) as the external standard. FTIR spectra were recorded using a Bruker Tensor 27 FTIR spectrophotometer and the conventional KBr disk method; 32 scans were collected at a spectral resolution of 4 cm^{-1}. The films used in this study were sufficiently thin to obey the Beer–Lambert law. Mass spectra were obtained using a Bruker Daltonics Autoflex MALDI-TOF mass spectrometer. The following voltage parameters were used: ion source 1, 19.06 kV; ion source 2, 16.61 kV; lens, 8.78 kV; reflector 1, 21.08 kV; reflector 2, 9.73 kV. The molecular weight of Pyridine-NH_2 was recorded using a Bruker Solarix high resolution Fourier Transform Mass spectroscopy system FT-MS (Bruker, Bremen, Germany). Molecular weight and molecular distributions of Pyridine-PTyr were determined through gel permeation chromatography (GPC) using a Waters 510 high performance liquid chromatography (HPLC) system equipped with a 410 differential refractometer and three ultrastyragel columns (500, 580, and 10 Å) connected in series, with DMF as the eluent (flow rate: 0.4 mL min^{-1}). DSC analyses were performed using a TA Q-20 differential scanning calorimeter operated under N_2 atmosphere. The sample (*ca.* 5–7 mg) was placed in a sealed aluminum sample pan and heated from 25 to 200 °C at a heating rate of 20 °C min^{-1}. A wide-angle X-ray diffraction (WAXD) pattern was obtained from the wiggler beamline BL17A1 of the National Synchrotron Radiation Research Center (NSRRC), Taiwan. A triangular bent Si (111) single crystal was used to obtain a monochromated beam with a wavelength (λ) of 1.33 Å. The samples were annealed at 180 °C for 2 h, and then cooled to room temperature before being measured by WAXD. UV-vis absorption spectra were recorded with an ocean optics DT 1000 CE 376 spectrophotometer. A small quartz cell with dimensions of 0.2 × 1.0 × 4.5 cm^3 was used to accommodate the solution sample and the concentration of the samples in the organic solvent was 10^{-4} M. PL was obtained from a LabGuide X350 fluorescence spectrometer using a 450 W Xe lamp as the continuous light source. Quantum yields (Φ_f) of the Pyridine-NH_2 and Pyridine-PTyr solutions were determined by using a quinine sulfate as the standard solution and the quantum efficiency (Φ_f) of the solid samples and polymer blends (Pyridine-PTyr–P4VP) were measured in an integrated sphere by ocean optics. Fluorescence lifetime measurements were performed by a HITACHI F-4500 fluorescence spectrometer with a light source of a 150 W XENON lamp. The PL lifetimes of solid state Pyridine-NH_2 and Pyridine-PTyr were measured at emitting bands of 500 nm with excitation wavelengths of 350 nm.

Results and discussion

Pyridine-NH_2 synthesis

Scheme 1 shows the synthesis of the diamine compound containing a pyridine heterocyclic ring, 2,6-bis(4-aminophenyl)-4-phenyl pyridine (Pyridine-NH_2). The dinitro compound containing a pyridine heterocyclic ring (Pyridine-NO_2) was prepared through a facile Chichibabin reaction.[31] The condensation of benzaldehyde with *p*-nitroacetophenone in the presence of ammonium acetate at reflux in glacial acetic acid obtained the dinitro-containing pyridine.[30] Next, the reduction of pyridine dinitro in absolute ethanol with hydrazine monohydrate in the presence of catalytic amounts of palladium on activated carbon at 80 °C was used to obtain the diamine compound (Pyridine-NH_2). Both FTIR and NMR spectroscopies confirmed the structure of these compounds. Fig. 1(a) and 1(b) show the FTIR spectra of Pyridine-NO_2 and Pyridine-NH_2, respectively. We can clearly observe the signals at 1525 and 1345 cm^{-1} due to the NO_2 group, while the signals at 3472 and 3379 cm^{-1} are due to NH stretching vibrations in the Pyridine-NH_2 compound. The proton NMR spectra in Fig. 2(a) and 2(b) indicate the formation of the pyridine heterocyclic group, as deduced from the chemical shifts at 7.99 ppm for the diamine compound and new signals appeared in the ^{1}H-NMR spectra at 5.40 ppm due to the amino group. Additionally, Fig. 3(a) and 3(b) present the ^{13}C-NMR spectra of Pyridine-NO_2 and Pyridine-NH_2, respectively. The carbon resonance signal of C2 in Pyridine-NO_2 appeared at 119.00 ppm, while the signal of the carbon resonance of C2 in Pyridine-NH_2 was shifted to 115.20 ppm. The FT-MS spectrum displays the molecular weight $[M + H]^+$ for Pyridine-NH_2, which is consistent with the predicted molecular weight as shown in Fig. S3.† These results confirm that we obtained a highly pure diamine compound that contains pyridine (Pyridine-NH_2).

Synthesis of Pyridine-PTyr by ring opening polymerization (ROP) of Tyr-NCA

Pyridine-PTyr was easily prepared *via* the diamine containing a pyridine heterocyclic ring initiated ring-opening polymerization (ROP) of L-tyrosine *N*-carboxyanhydride at room temperature.[32] Fig. 1(c) and 1(d) present the FTIR spectra of the Tyr-NCA monomer and the Pyridine-PTyr polymer. FTIR spectroscopy showed the characteristic anhydride peaks at (a) 1850 and (b) 1772 cm^{-1}, which are assigned to the two typical C=O stretching vibrations in the Tyr-NCA monomer. Using Pyridine-NH_2 as the initiator, the ring-opening polymerization of Tyr-NCA was performed in DMF as the solvent at room temperature for 72 h. After ROP of the NCA monomer, the FTIR spectra as depicted in Fig. 1(d) revealed the appearance of characteristic absorption peaks due to the peptide bands in the polymer backbone at 1652, 1626 (c) and 1531 (d) cm^{-1}.[21] Fig. 2(c) shows the ^{1}H-NMR spectrum of the Tyr-NCA monomer in DMSO-d_6. The singlet of the proton on the nitrogen atom (NH) and OH group appeared at 9.34 and 9.04 ppm, respectively. The resulting Pyridine-PTyr was analyzed *via* ^{1}H NMR and the spectrum in Fig. 2(d) clearly shows the characteristic peak signals of the NH proton (8.05 ppm), the phenolic OH protons (9.24 ppm), the COCHNH backbone (4.66 ppm) and the CH_2 protons (2.49 ppm). Fig. 3 (c) presents the ^{13}C-NMR spectrum of the tyrosine monomer in DMSO-d_6: the characteristic signals of the C=O carbon atoms (172.54, 152.02), the phenolic C–OH carbon atoms (154.44 ppm), the

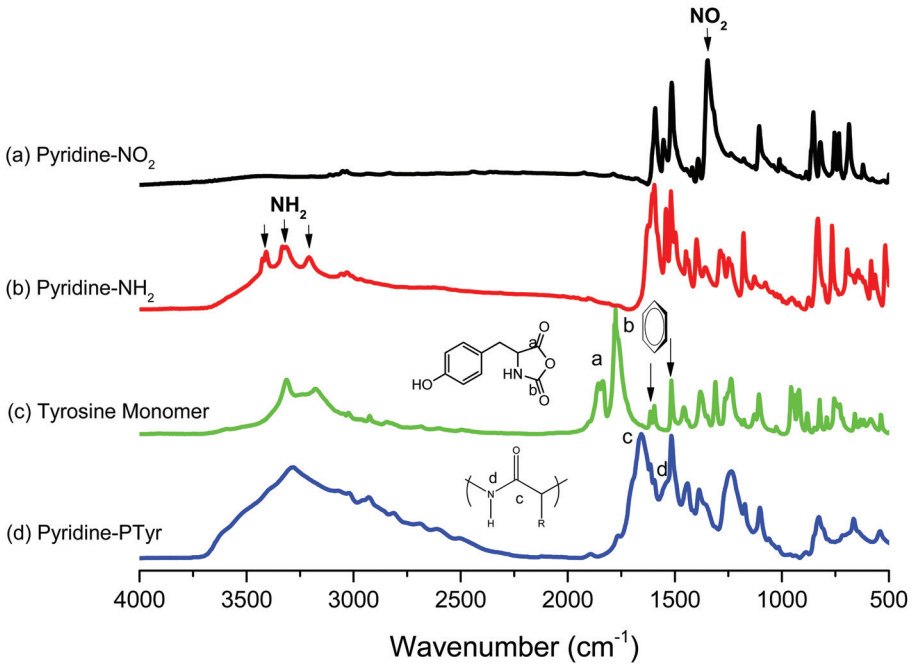

Fig. 1 FTIR spectra of (a) Pyridine-NO_2, (b) Pyridine-NH_2, (c) tyrosine monomer and (d) Pyridine-PTyr, recorded at room temperature.

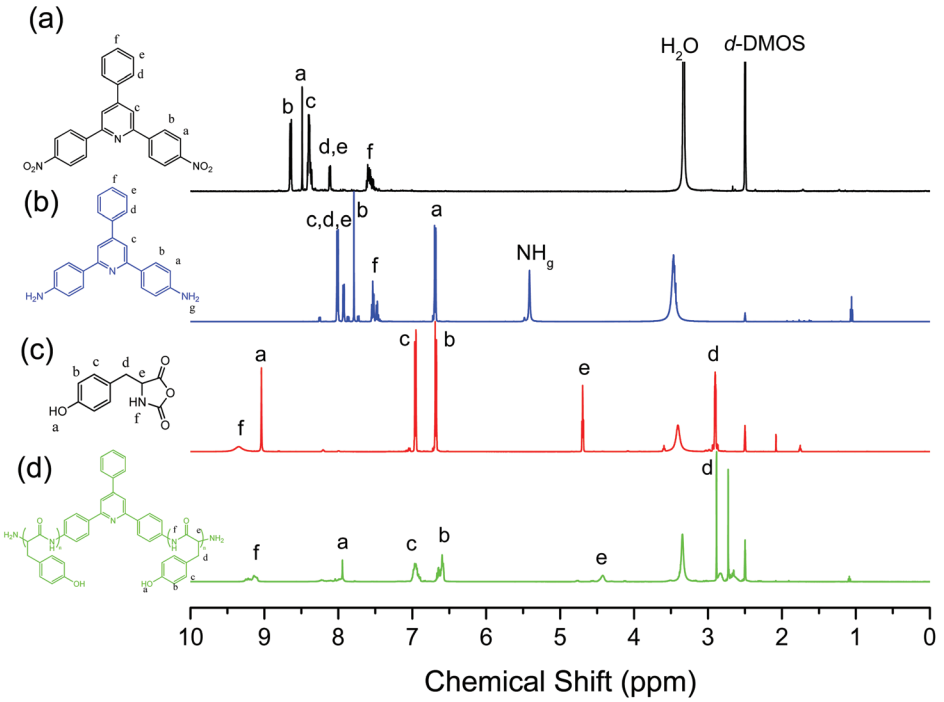

Fig. 2 ^{1}H NMR spectra of (a) Pyridine-NO_2, (b) Pyridine-NH_2, (c) tyrosine monomer and (d) Pyridine-PTyr.

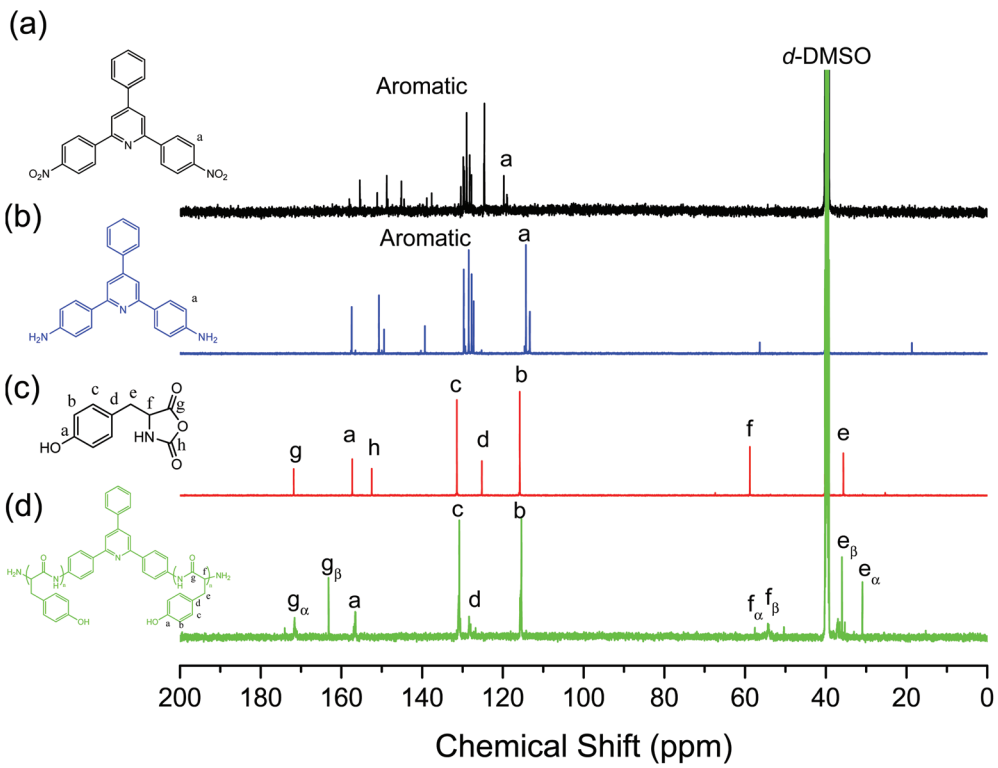

Fig. 3 ^{13}C NMR spectra of (a) Pyridine-NO_2, (b) Pyridine-NH_2, (c) tyrosine monomer and (d) Pyridine-PTyr.

benzyl carbon atom and the amino acid α-carbon atoms (NHCOC) (35.05, 58.88 ppm) of the tyrosine monomer. Fig. 3 (d) displays the ^{13}C-NMR spectrum of the Pyridine-PTyr in DMSO-d_6, revealing that the C═O and amide carbon atoms signals appeared in the Pyridine-PTyr at 171 and 162.6 ppm, respectively. The chemical shift at 55.65 ppm is ascribed the

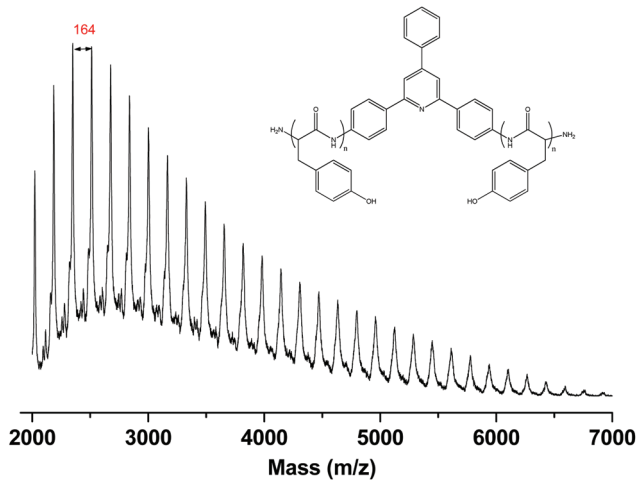

Fig. 4 MALDI-TOF mass spectrum of Pyridine-PTyr.

amino acid α-carbon atoms. Fig. 4 presents the MALDI-TOF mass spectrum of Pyridine-PTyr. Clearly, the mass difference between all adjacent peaks for Pyridine-PTyr is m/z 164 for a tyrosine repeating unit. Together, our results for ^{1}H, ^{13}C-NMR, FTIR spectroscopic analyses and MALDI-TOF mass spectrum confirmed the successful synthesis of Pyridine-PTyr (M_n = 3416 Da, PDI = 1.10).

Solvent effect of Pyridine-NH_2 and Pyridine-PTyr

Initially, to elucidate the solvatochromism effect, the photophysical properties of Pyridine-NH_2 and PTyr-Pyridine were investigated by absorption and emission spectroscopy at ambient temperature in different polar solvents. Pyridine-NH_2 exhibited good solubility in methanol, dichloromethane, acetone, THF, DMF and DMSO, while PTyr-Pyridine was soluble in methanol, DMF and DMSO and insoluble in acetone, DCM and THF. As depicted in Fig. 5(A), the Pyridine-NH_2 absorption spectra indicate that the absorption band varied depending on the nature of the solvent; this effect can be assigned to the π–π* transition. For example, Pyridine-NH_2 showed the absorption band at 290 nm in methanol, 292 nm in dichloromethane, 303 nm in DMF and 310 nm in DMSO. The absorption band of Pyridine-NH_2 was red shifted to 333 nm in acetone due to strong guest–host interactions between the molecule and the acetone environment. On the other hand, the absorption peak of Pyridine-NH_2 in methanol shifted to lower wavelengths because the fluorophore in the ground state is more stabilized compared to the excited state and may lead to form complexes with smaller length conjugations. The absorption behaviour of the Pyridine-NH_2 monomer is strongly dependent on solvent polarity.[26]

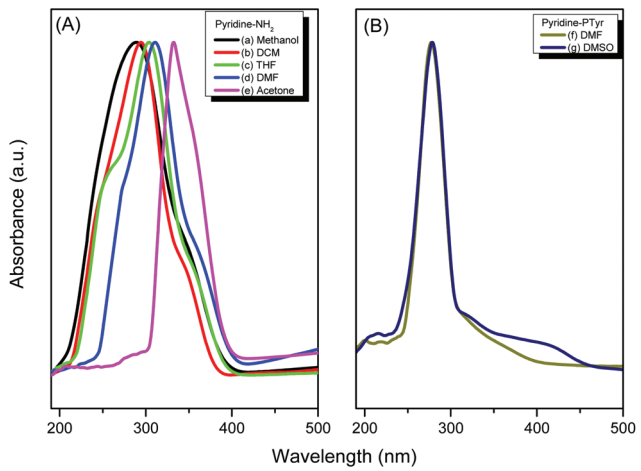

Fig. 5 UV-vis absorption spectra of (A) Pyridine-NH_2 and (B) Pyridine-PTyr at a concentration of 10^{-4} M.

Fig. 5(B) shows the absorption spectra of Pyridine-PTyr in DMF and DMSO. The high energy band (277 nm) has been assigned as the π–π* transition attributed to the phenyl group in the tyrosine and triphenyl pyridine units in both DMF and DMSO, respectively. To obtain further insight in the characteristics of the emissions from Pyridine-NH_2 and Pyridine-PTyr, it is necessary to do a series of experiments in the solution and solid states. Fig. 6(A) presents the Pyridine-NH_2 fluorescence emission spectra measured in solvents with different polarities, such as methanol, acetone, DCM, THF, DMSO and DMF. Interestingly, Pyridine-NH_2 shows emission peaks at 497 and 500 nm in DMF and DMSO, which correspond to the π–π* transition. When the solvent polarity increases from DCM to DMF, Pyridine-NH_2 is stabilized by the greater polarity that is found in DMSO and DMF due to the strong hydrogen bond interactions. We also investigated the Pyridine-PTyr fluorescence properties in methanol, DMF and DMSO, as shown in Fig. 6(B). The Pyridine-PTyr fluorescence emission peaks are located at 519, 496 and 505 nm in methanol, DMF and DMSO, respectively. The absorption and emission results show that Pyridine-NH_2 exhibits the solvatochromism effect, while Pyridine-PTyr did not show the solvatochromism effect. Fig. 7 presents the fluorescence emission spectra of Pyridine-NO_2, Pyridine-NH_2 and Pyridine-PTyr in the solid state. Pyridine-NO_2 does not exhibit any emission peaks, while Pyridine-NH_2 shows two fluorescence emission peaks at 436 nm due to monomer emission and at 486 nm corresponding to the excimer emission. Interestingly, Pyridine-PTyr displays a very strong emission peak at 536 nm and a bathochromic shift as shown in Fig. 7. Therefore, we carefully performed further experiments to prove these interesting phenomena and to report for the first time on the properties of the triphenyl pyridine functionalized-polytyrosine as the AIE unit in the polymer centre (Pyridine-PTyr). In order to investigate the optical properties of Pyridine-NH_2 and Pyridine-PTyr with solvent molecules, the quantum yields (Φ_f) of Pyridine-NH_2 and Pyridine-PTyr in solution were measured by using quinine sulfate in 1 N H_2SO_4 (Φ_f = 0.55) as the standard. The quantum yield results are summarized in Table S1.† In addition, the quantum efficiencies (Φ_f) of Pyridine-NH_2 and Pyridine-PTyr in the solid state were 25.8 and 38.3%, respectively. The values of fluorescence lifetime for Pyridine-NH_2 and Pyridine-PTyr in

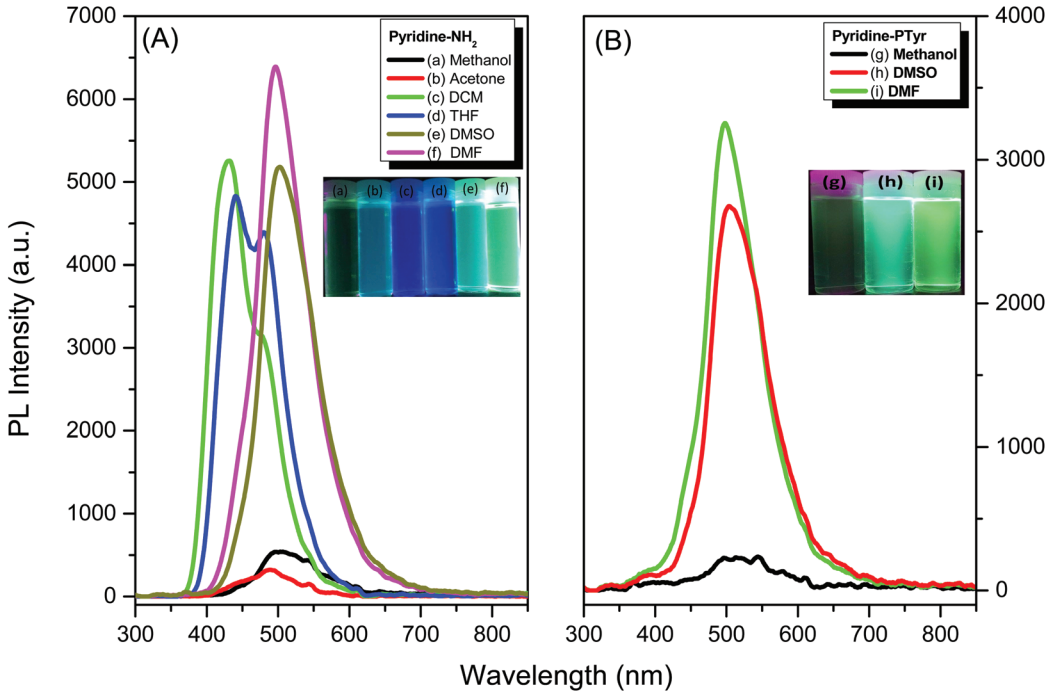

Fig. 6 Photoluminescence spectra of (A) Pyridine-NH_2 and (B) Pyridine-PTyr at a concentration of 10^{-4} M.

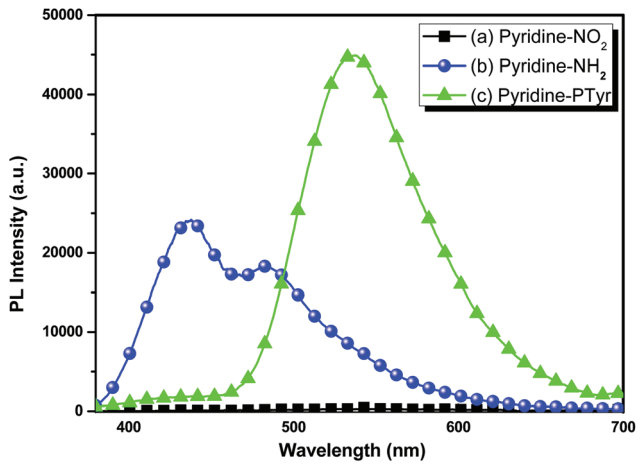

Fig. 7 Photoluminescence spectra of (A) Pyridine-NO_2, (B) Pyridine-NH_2 and (C) Pyridine-PTyr in the solid state with excitation wavelength 350 nm.

the solid state were τ_1 = 0.14 ns, τ_1 = 0.13 and τ_2 = 9.24 ns, respectively, based on Fig. S5.†

Aggregation-induced emission (AIE) phenomena

As mentioned above, most organic emissive materials exhibit a high emission in solution but quenched emissions in concentrated solutions and the aggregate (solid) state. This type of emission quenching is due to noncovalent intramolecular interactions such as π–π stacking and is known as aggregation-caused quenching (ACQ). Our first question was whether our Pyridine-NH_2 (initiator) and Pyridine-PTyr (polymer) exhibit aggregation-induced emission (AIE) or not. We carefully investigated the AIE features of Pyridine-NH_2 and Pyridine-PTyr using the concentration effect and solvent pairs. Fig. 8 shows the concentration effect of the fluorescence emission of Pyridine-NH_2 and Pyridine-PTyr. Fig. 8(A) shows that the emission intensity decreased by increasing the Pyridine-NH_2 concentration in the DMF solution. The concentration-quenched emission is observed for Pyridine-NH_2 due to the intramolecular π–π interaction and formation of an excimer. Fig. 8(B) shows the concentration effect on the emission behavior of Pyridine-PTyr. As shown in Fig. 5(B), the dilute solu-

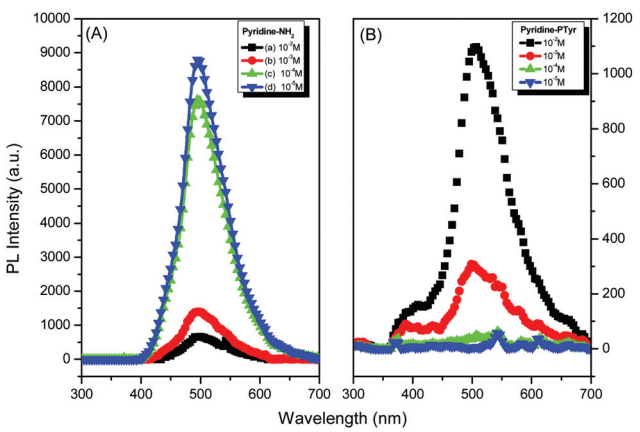

Fig. 8 Photoluminescence spectra of (A) Pyridine-NH_2 (DMF) and (B) Pyridine-PTyr (Methanol) with excitation wavelength 350 nm.

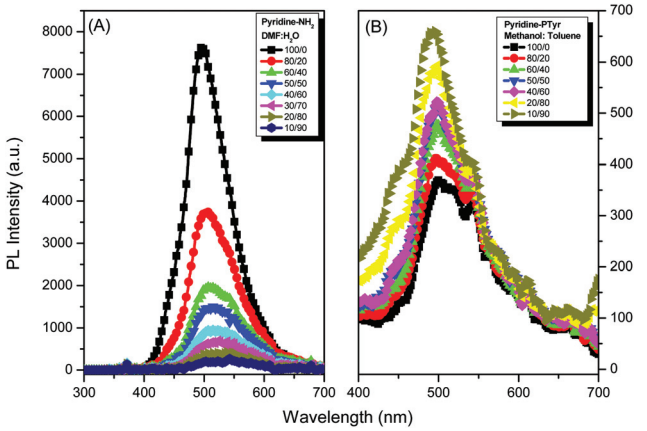

Fig. 9 Photoluminescence spectra of (A) Pyridine-NH_2 in the DMF–water and (B) Pyridine-PTyr in methanol–toluene with the concentration 1×10^{-4} M under a 350 nm irradiation.

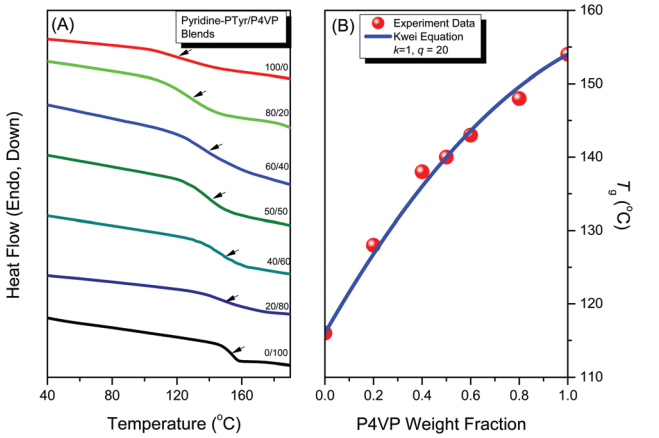

Fig. 10 (A) DSC traces (third heating run) of Pyridine-PTyr–P4VP blends and (B) T_g plot of Pyridine-PTyr with an increasing P4VP content.

tion of Pyridine-PTyr 10^{-5} M contains very small amounts of fluorophore and showed a very weak emission. However, by increasing the Pyridine-PTyr concentration from 10^{-4} to 10^{-2} M, the emission intensity continuously increased in the methanol solution. The concentration-enhanced emission observed for the Pyridine-PTyr methanol solution ish ascribed to the AIEE effect. Based on these rather interesting results, we strongly suggest that emission in Pyridine-NH_2 is transformed from aggregation-caused emission to AIEE by attachment to the rigid polytyrosine backbone. To further demonstrate the ACQ for Pyridine-NH_2, Pyridine-NH_2 behavior in solvent-non solvent DMF–water was studied as shown in Fig. 9(A). In this study, we observe that the dilute Pyridine-NH_2 solution (10^{-4} M) in DMF emitted strongly at 520 nm. Furthermore, the fluorescence emission decreased by increasing the water concentration and was quenched up to 90%. In this study we did not select DMF as the good PTyr-Pyridine solvent to avoid the strong hydrogen bond interaction between the C═O group in DMF and the phenolic OH in polytyrosine. Interestingly, while preparing the stock solution of Pyridine-PTyr in methanol as the good solvent by varying the toluene (as the poor solvent) concentration, we determined that the fluorescence emission was enhanced because of their aggregate nature. Hence, we performed the AIEE analysis. As shown in Fig. 9(B), the PL intensities were enhanced by increasing the concentration of toluene (up to 90%). From these further experiments, we confirmed that the new PTyr-Pyridine fluorescent material exhibits AIE while Pyridine-NH_2 is an ACQ material.

Hydrogen bonding interactions between Pyridine-PTyr–P4VP blends

Thermal analyses of Pyridine-PTyr–P4VP blends. The DSC technique was used to perform the thermal analysis of Pyridine-PTyr in the pure state and its miscibility after blending with different weight ratios of poly(4-vinylpyridine) through mediated intermolecular hydrogen bonding in a DMF solution as shown in Fig. 10. Fig. 10(A) shows that the glass transition temperature of pure Pyridine-PTyr used in this study was only lower than that of pure linear PTyr (155 °C);[21] this finding was attributed to the bowl-shaped corannulene ring and the non-coplanar triphenylpyridine unit that increase the free volume and subsequently decrease the T_g behaviour. Clearly, a single T_g behaviour was found for PTyr-Pyridine–P4VP blends, indicating the total miscibility of this blend system. Moreover, in Fig. 10(B), the glass transition temperatures for the Pyridine-PTyr–P4VP blends increased with increasing P4VP content due to hydrogen bonding interactions between pairs of electrons on the N atoms in the pyridine groups of P4VP and the phenolic OH of Pyridine-PTyr. Additionally, we obtained the values of k and q of 1 and 20, respectively, for Pyridine-PTyr–P4VP blends based on the Kwei equation.[33] The positive q value implies that inter-association interactions between Pyridine-PTyr–P4VP is stronger than the self-association of Pyridine-PTyr. The conclusion from these results is that the Pyridine-PTyr–P4VP blend system shows that the random coils are separated.

Conformation transition and hydrogen bonding interaction of Pyridine-PTyr–P4VP blends in the bulk state. FTIR spectroscopy provides a simple, quick and facile method to investigate the non-covalent interactions between poly(4-vinylpyridine) and Pyridine-PTyr; we also studied the secondary structure conformations of Pyridine-PTy–/P4VP blends in the solid state at room temperature. The hydrogen bonding between the pyridine ring and phenolic OH groups in Pyridine-PTyr was investigated by FTIR spectroscopy as shown in Fig. 11. The hydrogen bond acceptance of P4VP can be monitored by observing the shifts of the pyridine ring modes at 993 cm^{-1},[34] as shown in Fig. 11(B). Indeed, this finding clearly exhibits band shifts of the lowest wavenumber from 993 to 1005 cm^{-1};[35,36] it is possible to use two absorption peaks to analyze the specific interaction by subtracting the signal for pure Pyridine-PTyr at 1015 cm^{-1} based on the weight fraction of Pyridine-PTyr in these blends as shown in Fig. 12(B).

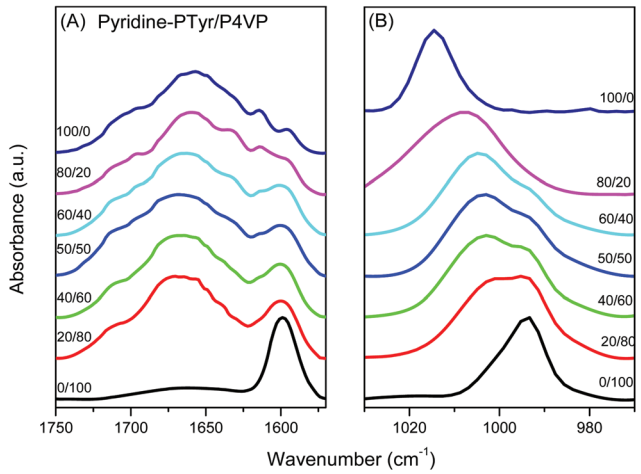

Fig. 11 FTIR spectra recorded at ambient temperature, displaying the region between 1750–1580 cm^{-1} (A) and the region between 1030 and 970 cm^{-1} (B) for PTyr-Pyridine–P4VP blends.

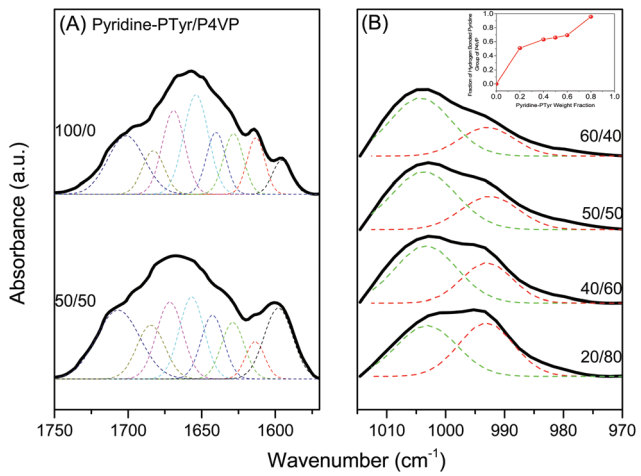

Fig. 12 Curve fitting of the signals in the FTIR spectra of Pyridine-PTyr–P4VP blends of (A) the amide I group and (B) the pyridine group and the inset figure for the fraction of hydrogen bonded pyridine group with various Pyridine-PTyr compositions.

Clearly, the fraction of hydrogen-bonded Pyridyl groups increased with the increase of Pyridine-PTyr weight fraction as shown in the inset of Fig. 12(B).

As mentioned in the introduction part, the secondary structures of the polypeptide are strongly dependent on the degree of polymerization, DP. For example, Pakula *et al.* reported that the α-helical secondary structure of PBLG is favored at a degree of polymerization >18.[37] As shown in Fig. 12(A), in this study we observed major peaks for pure Pyridine-PTyr using the second-derivative technique: 1597 and 1615 cm^{-1} for the ring vibrations of tyrosine; 1655 cm^{-1} for the α-helical conformation; 1630 cm^{-1} for the β-sheet conformation; 1670 cm^{-1} for the β-turn conformation; and 1643, 1683 and 1700 cm^{-1} for the random coil conformation. Clearly, when blended with a 50 wt% ratio of P4VP, the secondary structure (α-helical and

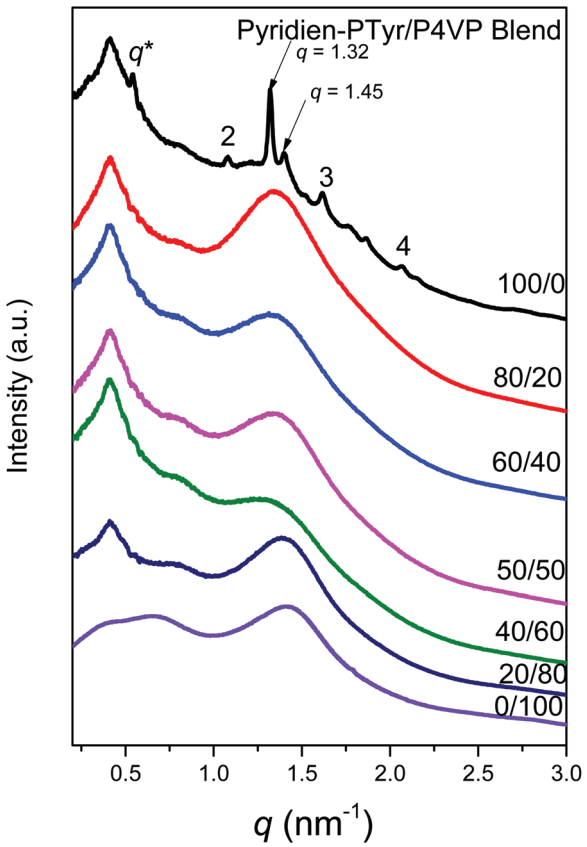

Fig. 13 WAXD patterns of the Pyridine-PTyr–P4VP blends.

β-sheet) conformations decreased and the fraction of random coil conformations increased from 37.2% to 42.4%.

To further elucidate the changes in the secondary structures of the Pyridine-PTyr–P4VP blends, WAXD experiments were performed at room temperature as provided in Fig. 13. In Fig. 13, Bragg's diffraction pattern showed the presence of β-sheet secondary structures for pure Pyridine-PTyr (DP = 10).

For more details, we can observe the signature of the first such structure at q = 0.54 (d = 1.15 nm), corresponding to the distance between the backbones in the antiparallel β-pleated sheet structure. The diffraction peak centered at q = 1.32 (corresponding to d = 0.475 nm) is observed, indicating the intermolecular distance between adjacent peptide chains within one lamella.[38] Clearly, the secondary structure β-sheet conformation has disappeared, and as shown the diffraction patterns of Pyridine-PTyr become a broad amorphous halo after increasing the P4VP content in the Pyridine-PTyr–P4VP blend system.[21]

Emission properties of Pyridine-PTyr–P4VP blends in the solid state. As mentioned above, Pyridine-PTyr showed an aggregation-induced emission phenomena and a notably high fluorescence emission intensity. Interestingly, after blending with P4VP (20, 40, 50 wt%), the Pyridine-PTyr emission intensity decreased and a hypsochromic shift from 536 to 489 nm was observed (Fig. 14); this was attributed to the hydrogen

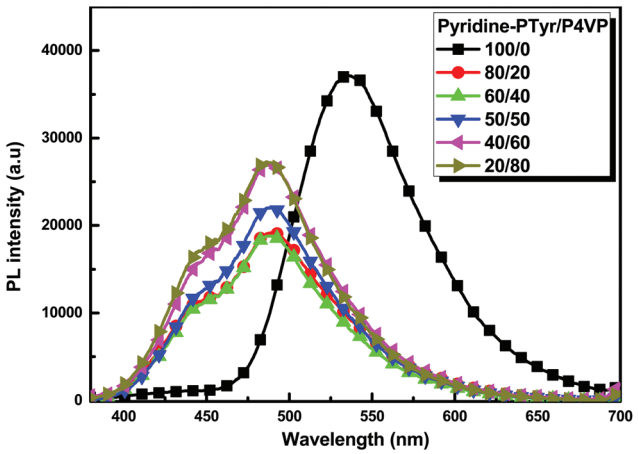

Fig. 14 Photoluminescence spectroscopy of Pyridine-PTyr–P4VP blends in solid state under a 350 nm irradiation.

bonding interaction between P4VP and the phenolic OH groups of PTyr and the release of the restricted intramolecular rotation of the triphenyl pyridine unit in the center of the polymer. When the P4VP content increased (up to 60, 80 wt%), the fluorescence intensities increased gradually because of the restricted intramolecular rotation of the triphenyl pyridine unit, while the PL emission peak still exhibited the hypsochromic shift. We also measured the quantum efficiency (Φ_f) in the solid state and the values were 38.3, 32.8, 32.8, 34.8 and 35.4 for 20, 40, 50 and 60 wt% of P4VP in the Pyridine-PTyr–P4VP blend system. We also measured the temperature-dependent fluorescence of a Pyridine-PTyr–P4VP blend (40/60) to investigate the role of hydrogen bonding interactions in this study. As shown in Fig. S6,† the emission intensity of Pyridine-PTyr–P4VP remained the same without any changes at a temperature between 25 and 60 °C, which is attributed to the restricted intramolecular rotation of the blend. However, a decreasing emission intensity of Pyridine-PTyr–P4VP was observed at temperatures from 80 to 160 °C because of the release of the intramolecular rotation and dissociation of intermolecular hydrogen bonding between the phenolic hydroxyl groups in the polytyrosine chain and the pyridine ring in P4VP.

Conclusions

In this report, the synthetic route of Pyridine-PTyr homopolymer through ROP of L-tyrosine-*N*-carboxyanhydride using Pyridine-NH_2 as the initiator with controlled PDI was described and tested. We carefully confirmed its chemical structure using FTIR, ^{1}H and ^{13}C NMR, and MALDI-TOF mass spectroscopies. Interestingly, the PL results revealed that while Pyridine-NH_2 was an ACQ material, it became a strongly AIE material after attachment to rigid-rod polytyrosine due to the restriction of the intramolecular rotation (RIR) mechanism. DSC analysis revealed that the glass transition temperature of Pyridine-PTyr (120 °C) was lower than that of the pure linear polytyrosine (155 °C) due to its bowl-shaped corannulene ring and non-coplanar triphenylpyridine unit. We determined that the emission intensity of Pyridine-PTyr was decreased and that a hypsochromic shift from 536 to 489 nm was observed due to the release of the restricted intramolecular rotation of the triphenyl pyridine unit in the center of the polymer caused by the intermolecular hydrogen bonding of PTyr with P4VP; this conclusion was based on the results of IR spectroscopy, while the separated random coils behavior of the Pyridine-PTyr chains was deduced from the analysis of the wide-angle X-ray diffraction.

Acknowledgements

This study was supported financially by the Ministry of Science and Technology, Taiwan, under contracts MOST103-2221-E-110-079-MY3 and MOST102-2221-E-110-008-MY3.

References

1 S. N. S. Alconel, S. A. Baas and D. H. Maynard, *Polym. Chem.*, 2011, **2**, 1442–1448.
2 A. H. Gauthier and A. H. Klok, *Chem. Commun.*, 2008, 2591–2611.
3 Y. Chen, H. X. Pang and M. C. Dong, *Adv. Funct. Mater.*, 2010, **20**, 579–586.
4 M. S. Peng, Y. Chen, C. Hua and M. C. Dong, *Macromolecules*, 2009, **42**, 104–113.
5 T. J. Deming, *Adv. Mater.*, 1997, **9**, 299–311.
6 X. Zhang, J. Li, W. Li and A. Zhang, *Biomacromolecules*, 2007, **8**, 3557–3567.
7 H. R. Kricheldorf, *Angew. Chem., Int. Ed.*, 2006, **45**, 5752–5784.
8 T. J. Deming, *Prog. Polym. Sci.*, 2007, **32**, 858–875.
9 P. Papadopoulous, G. Floudas, A. H. Klok, I. Schnell and T. Pakula, *Biomacromolecules*, 2004, **5**, 81–91.
10 N. Hadjichristidis, H. Iatrou, M. Pitsikalis and G. Sakellariou, *Chem. Rev.*, 2009, **109**, 5528–5578.
11 C. He, X. Zhuang, Z. Tang, H. Tian and X. Chen, *Adv. Healthcare Mater.*, 2012, **1**, 48–78.
12 H. Tang and D. Zhaung, *Biomacromolecules*, 2010, **11**, 1585–1592.
13 J. R. Kramer and T. J. Deming, *J. Am. Chem. Soc.*, 2012, **132**, 15068–15071.
14 C. Chen, Z. Wang and Z. Li, *Biomacromolecules*, 2011, **12**, 2859–2863.
15 X. Fu, Y. Shen, W. Fu and Z. Li, *Macromolecules*, 2013, **46**, 3753–3760.
16 Y. C. Lin and S. W. Kuo, *Polym. Chem.*, 2012, **3**, 162–171.
17 Y. C. Lin and S. W. Kuo, *Polym. Chem.*, 2012, **3**, 882–891.
18 Y. C. Lin, P. I. Wang and S. W. Kuo, *Soft Matter*, 2012, **8**, 9676–9684.

19 S. W. Kuo and C. J. Chen, *Macromolecules*, 2011, **44**, 7315–7326.
20 S. W. Kuo and C. J. Chen, *Macromolecules*, 2012, **45**, 2442–2452.
21 Y. S. Lu, Y. C. Lin and S. W. Kuo, *Macromolecules*, 2012, **45**, 6547–6556.
22 F. Y. Yan, M. Wang, D. L. Cao, N. Yang, Y. Fu, L. Chen and L. G. Chen, *Dyes Pigm.*, 2013, **98**, 42–50.
23 M. Xavier, P. Fabien, L. D. Thilo, D. Maxime, B. P. Marcel, A. A. Paul and W. Shimon, *Single Mol.*, 2001, **2**, 261–276.
24 S. Chenais and S. Forget, *Polym. Int.*, 2012, **61**, 390–406.
25 S. A. Jenekhe and J. A. Osaheni, *Science*, 1994, **265**, 765–768.
26 (*a*) R. H. Friend, R. W. Gymer, A. B. Holmes, J. H. Burroughes, R. N. Marks and C. Taliani, *Nature*, 1999, **397**, 121–128; (*b*) K. Y. Pu and B. Liu, *Adv. Funct. Mater.*, 2009, **19**, 277–284; (*c*) X. Zhang, M. Cui, R. Zhou, C. Chen and G. Zhang, *Macromol. Rapid Commun.*, 2014, **35**, 566–573; (*d*) G. Zhang, G. M. Palmer, M. W. Dewhirst and C. L. Fraser, *Nat. Mater.*, 2009, **8**, 747–751; (*e*) Y. Cao, W. Xi, L. Wang, H. Wang, L. Kong, H. Zhou, J. Wu and Y. Tian, *RSC Adv.*, 2014, **4**, 24649–24652; (*f*) M. S. Zakerhamidi, A. Ghanadzadeh and M. Moghadam, *Chem. Sci.*, 2012, **1**, 1–8; (*g*) G. Zhang, M. P. Aldred, W. L. Gong, C. Li and M. Q. Zhu, *Chem. Commun.*, 2012, **48**, 7711–7713.
27 (*a*) J. Luo, Z. Xie, J. W. Y. Lam, L. Cheng, H. Chen, C. Qiu, H. S. Kwok, X. Zhan, Y. Liu, D. Zhu and B. Z. Tang, *Chem. Commun.*, 2001, 1740–1741; (*b*) Z. Zhao, S. Chen, J. W. Y. Lam, P. Lu, Y. Zhong, K. S. Wong, H. S. Kwok and B. Z. Tang, *Chem. Commun.*, 2010, **46**, 2221–2223; (*c*) J. Liu, Y. Zhong, J. W. Y. Lam, P. Lu, Y. Hong, Y. Yu, Y. Yue, M. Faisal, H. H. Y. Sung, I. D. Williams, K. S. Wong and B. Z. Tang, *Macromolecules*, 2010, **43**, 4921–4936; (*d*) R. H. Chien, C. T. Lai and J. L. Hong, *Macromol. Chem. Phys.*, 2012, **213**, 666–677.
28 S. T. Li, Y. C. Lin, S. W. Kuo, W. T. Chuang and J. L. Hong, *Polym. Chem.*, 2012, **3**, 2393–2402.
29 K. Y. Shih, Y. C. Lin, T. S. Hsiao, S. L. Deng, S. W. Kuo and J. L. Hong, *Polym. Chem.*, 2014, **5**, 5765–5774.
30 C. H. Lin, Y. S. Shih, M. W. Wang, C. Y. Tseng, T. Y. Juang and C. F. Wang, *RSC Adv.*, 2014, **4**, 8692–8698.
31 R. L. Frank and R. P. Seven, *J. Am. Chem. Soc.*, 1949, **71**, 2629–2635.
32 G. J. M. Habraken, M. Peeters, C. H. J. T. Dietz, C. E. Koning and A. Heise, *Polym. Chem.*, 2010, **1**, 514–524.
33 T. K. Kwei, *J. Polym. Sci., Polym. Lett. Ed.*, 1984, **22**, 307–313.
34 S. W. Kuo, P. H. Tung and F. C. Chang, *Macromolecules*, 2006, **39**, 9388–9395.
35 J. Y. Lee, P. C. Painter and M. M. Coleman, *Macromolecules*, 1988, **21**, 954–960.
36 S. W. Kuo, C. L. Lin and F. C. Chang, *Polymer*, 2002, **43**, 3943–3949.
37 P. Papadopoulous, G. Floudas, A. H. Klok, I. Schnell and T. Pakula, *Biomacromolecules*, 2004, **5**, 81–91.
38 H. E. Auer and R. P. Mcknight, *Biochem*, 1978, **14**, 2793–2798.

